Electronic Supplementary Information

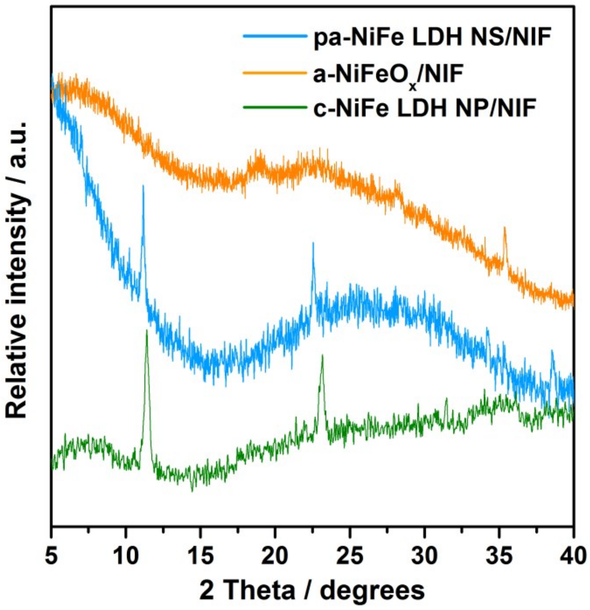

Fig. S1 XRD patterns of a-NiFeO$_x$/NIF, pa-NiFe LDH NS/NIF and c-NiFe LDH NP/NIF, from which the fully amorphous characteristics of a-NiFeO$_x$/NIF as well as the highly crystalline nature of c-NiFe LDH NP/NIF can be identified.

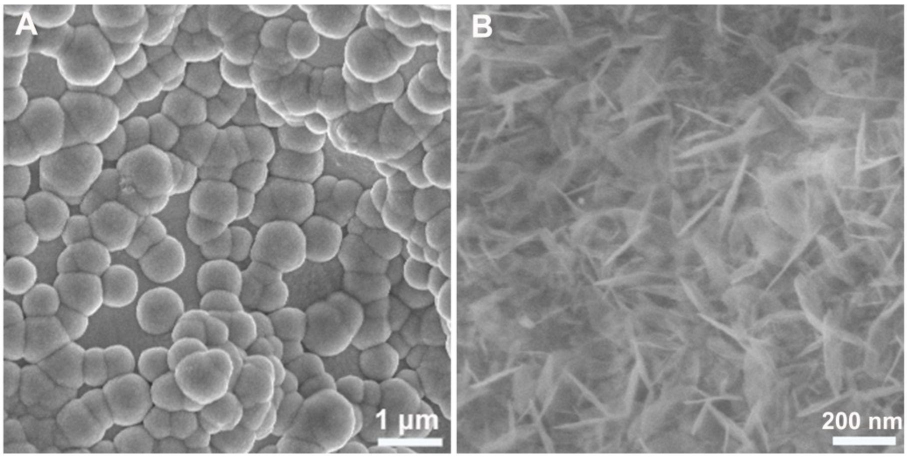

Fig. S2 SEM images of (A) a-NiFeO$_x$/NIF and (B) c-NiFe LDH NP/NIF. The fully amorphous a-NiFeO$_x$/NIF is shaped in spherical morphology, while the highly crystalline c-NiFe LDH NP/NIF shows a large lateral size of hundreds of nanometers with nanoplate thickness of ~20 nm.

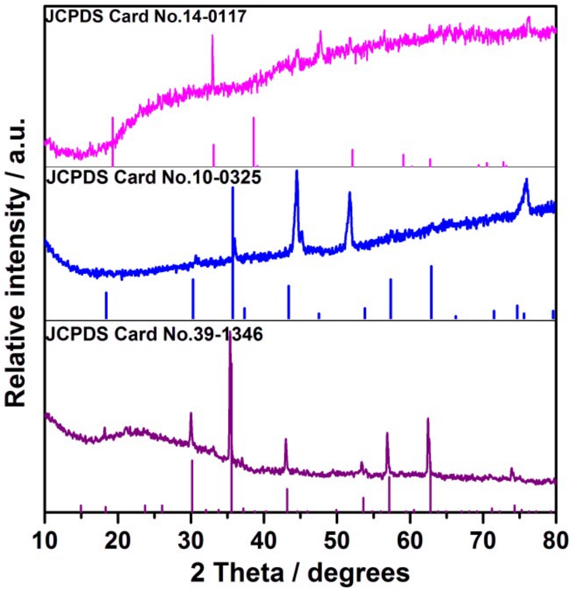

Fig. S3 XRD patterns of the counterparts with the standard patterns, where the top lilac pattern is $Ni(OH)_2$/NF, middle blue pattern is $NiFe_2O_4$ NP/NIF and the bottom purple pattern is γ-Fe_2O_3/IF.

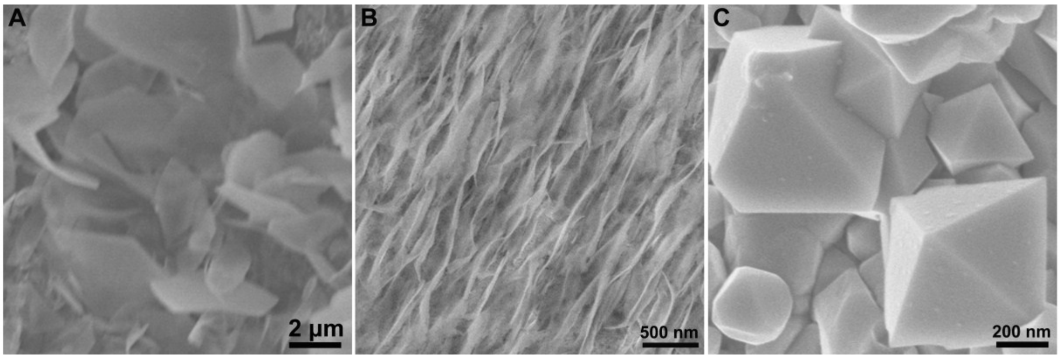

Fig. S4 SEM images of (A) $NiFe_2O_4$ NP/NIF, (B) $Ni(OH)_2$/NF and (C) γ-Fe_2O_3/IF.

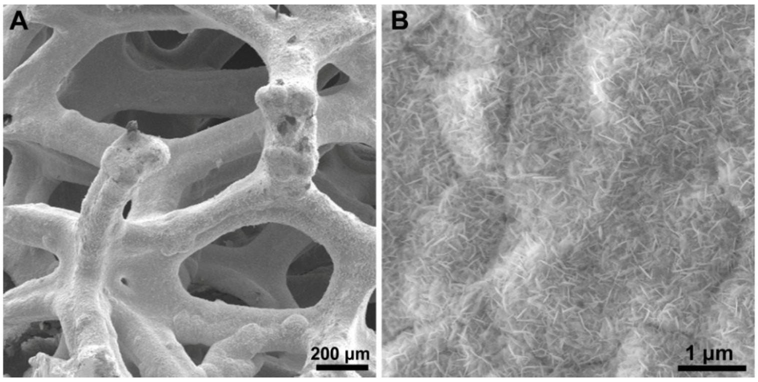

Fig. S5 SEM images of pa-NiFe LDH NS/NIF at low magnifications.

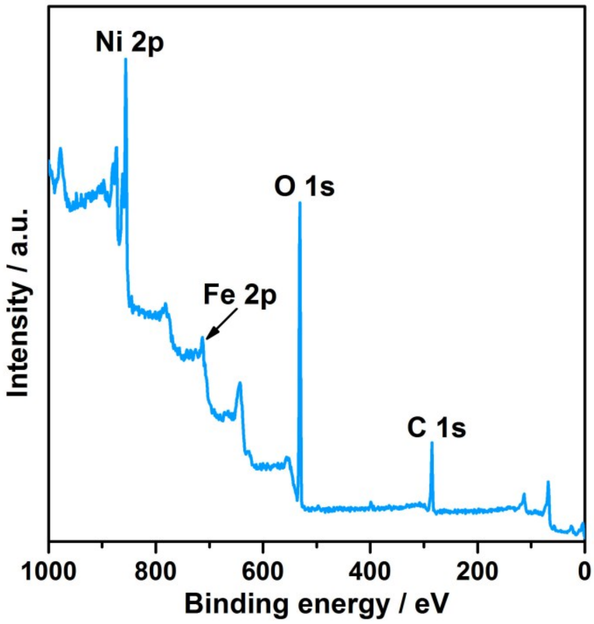

Fig. S6 XPS survey spectra of pa-NiFe LDH NS/NIF.

The estimation of the effective active surface area of the samples was carried out according to literature.[1] Cyclic voltammetry (CV) was performed at various scan rates (20, 40, 60 mV s^{-1}, etc.) in 1.0–1.1 V vs. RHE region. The electrochemical double-layer capacitance (C_{dl}) of various samples can be determined from the cyclic voltammograms, which is expected to be linearly proportional to the effective surface area (Fig. S7A-F). CV measurements were taking in the region of 1.0-1.1 V vs. RHE, which could be mostly considered as the double-layer capacitive behavior. The double-layer capacitance is estimated by plotting the ΔJ (J_a-J_c) at 1.05 V vs. RHE against the scan rate, where the slope is twice C_{dl}. The calculated values of double-layer capacitance are as follows: 2.02 mF cm^{-2}, 1.98 mF cm^{-2}, 1.62 mF cm^{-2}, 1.78 mF cm^{-2}, 1.55 mF cm^{-2}, 1.23 mF cm^{-2} for pa-NiFe LDH NS/NIF, a-NiFeO$_x$/NIF, c-NiFe LDH NP/NIF, $NiFe_2O_4$ NP/NIF, $Ni(OH)_2$/NF and γ-Fe_2O_3/IF, respectively. Analysis shows pa-NiFe LDH NS/NIF has a larger double-layer capacitance than the other counterparts. Therefore, similarly high C_{dl} values are identified, which indicates that ECSA is not the main reason for the enhanced OER and UOR activities of pa-NiFe LDH NS/NIF.

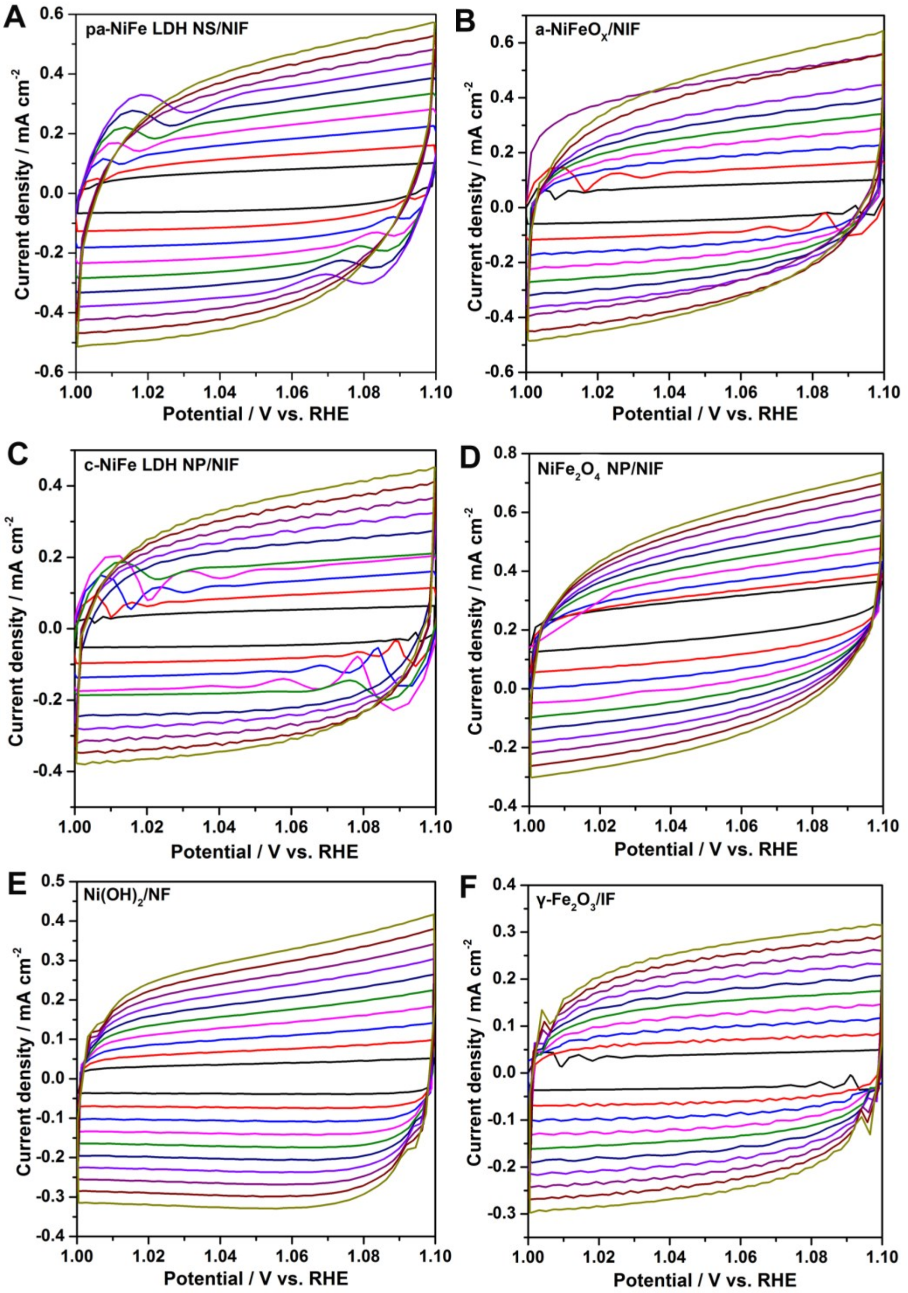

Fig. S7 CV curves of different catalysts at non-redox region for the calculation of electrochemical double-layer capacitance.

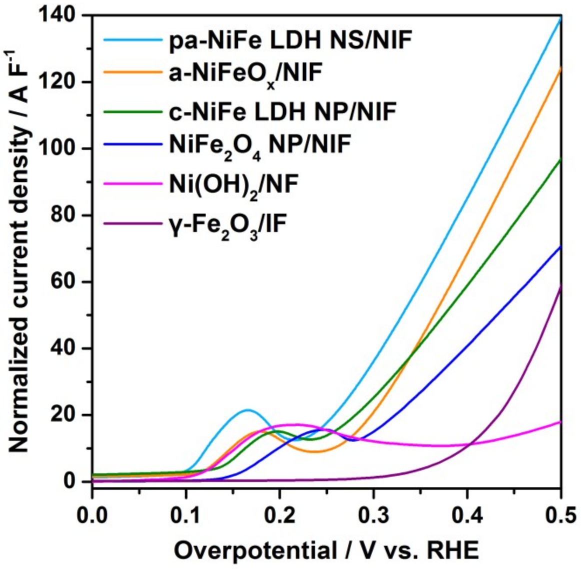

Fig. S8 C_{dl}-normalized OER currents with respect to the overpotential.

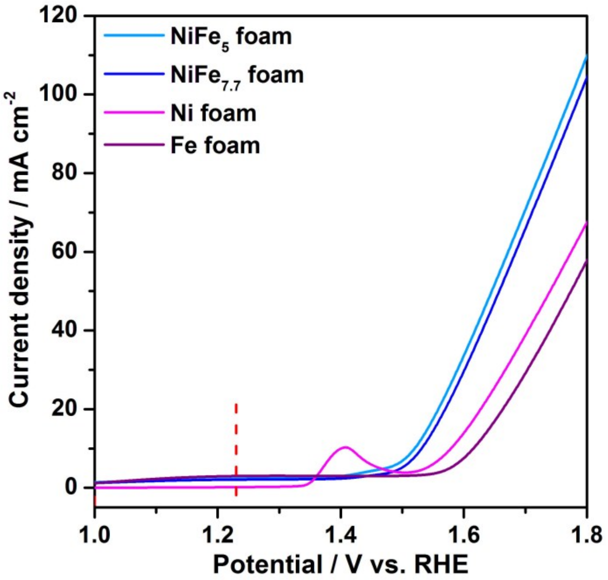

Fig. S9 LSV curves of various bare metal foams measured in 1 M KOH electrolyte.

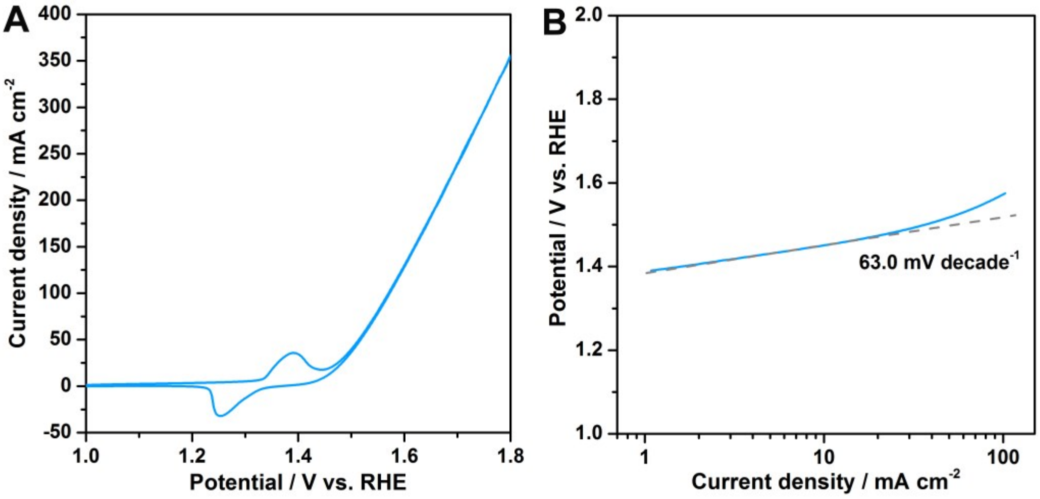

Fig. S10 (A) CV curve of pa-NiFe LDH NS/NIF. (B) Tafel plot of pa-NiFe LDH NS/NIF derived from the cathodic sweep of CV curve to avoid the interference of the oxidation peak.[2] The Tafel slope is calculated to be as small as 63.0 mV decade^{-1}.

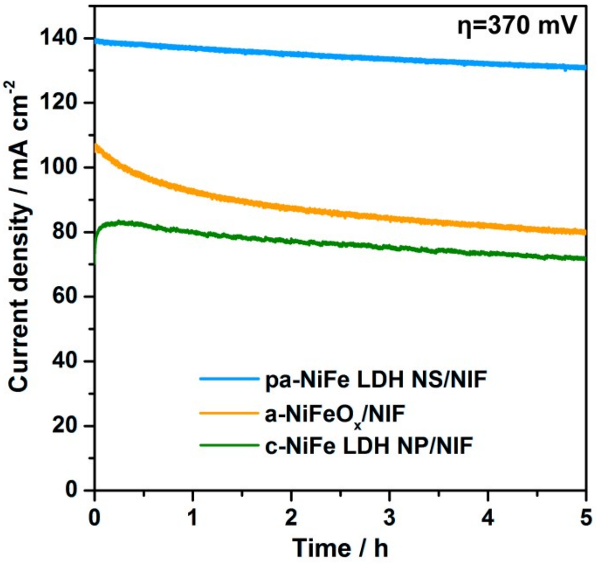

Fig. S11 Stability tests of pa-NiFe LDH NS/NIF, a-NiFeO$_x$/NIF and c-NiFe LDH NP/NIF in 1 M KOH under a fixed overpotential of 370 mV. The partially amorphous catalyst and the highly crystalline electrode exhibit high electrochemical stability with ~94.7% and 93.8% retention of anodic current after 5h continuous OER operation, while the fully amorphous catalyst shows rather poor stability which degrades for 26.5% after 5h OER test, which can be attributed to the higher solubility of the amorphous material.[3-5]

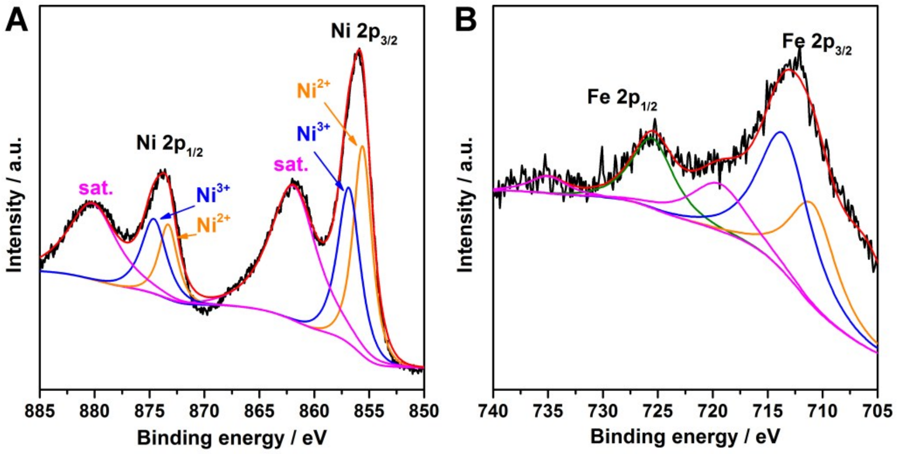

Fig. S12 XPS spectra of (A) nickel and (B) iron for of pa-NiFe LDH NS/NIF after 10 h continuous OER operation.

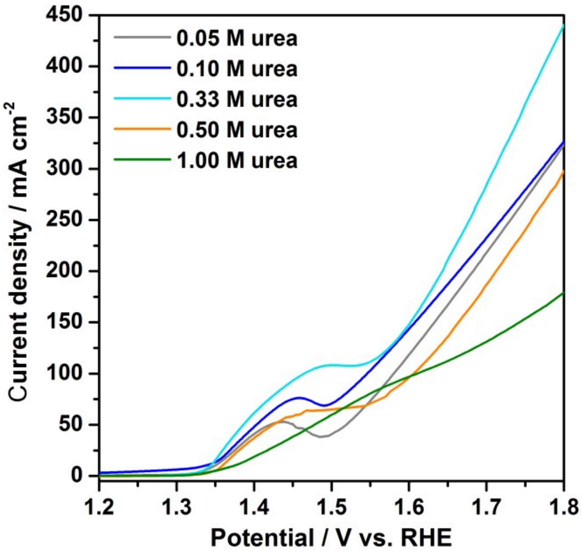

Fig. S13 LSV curves of the pa-NiFe LDH NS/NIF in 1 M KOH with various urea concentration.

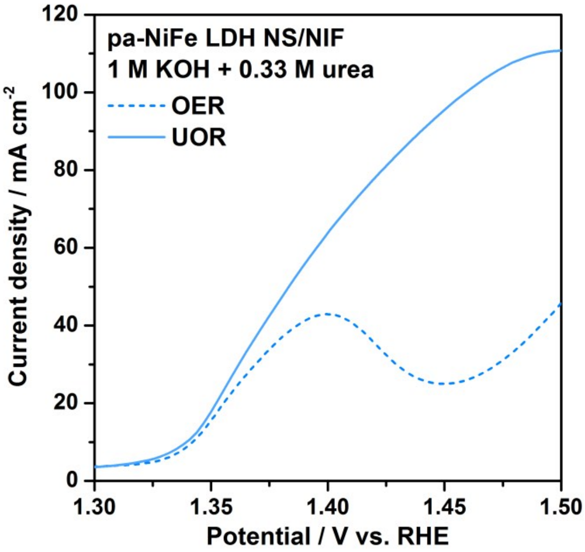

Fig. S14 Comparison of OER and UOR curves of pa-NiFe LDH NS/NIF at onset region.

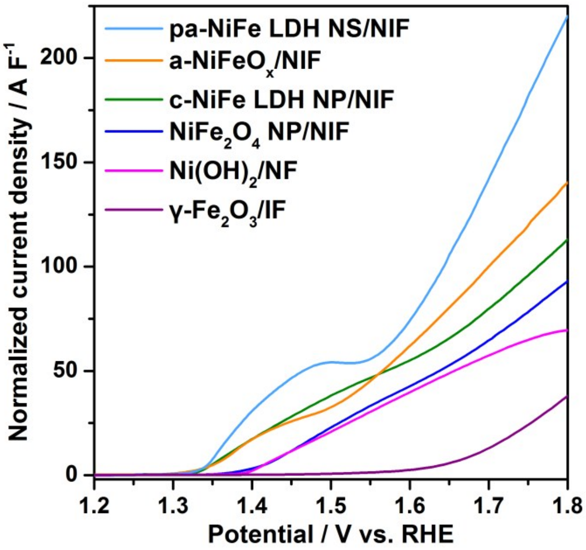

Fig. S15 UOR catalytic currents normalized by C_{dl} measured in mixed solution containing 1 M KOH and 0.33 M urea.

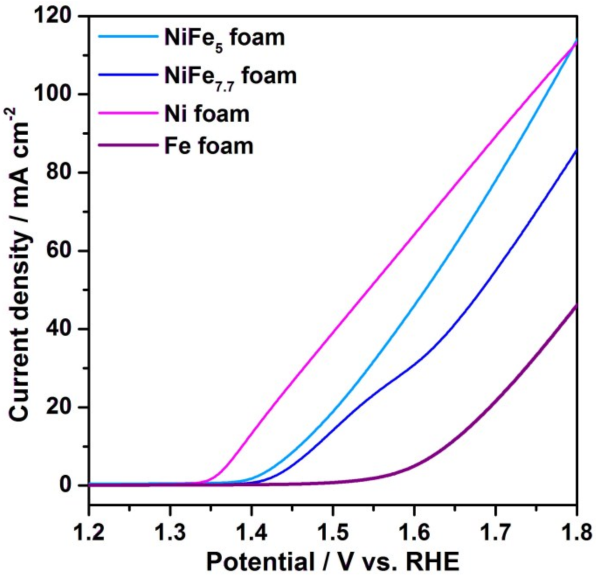

Fig. S16 Comparison of UOR performance of different bare metal foams measured in the mixed solution containing 1 M KOH and 0.33 M urea.

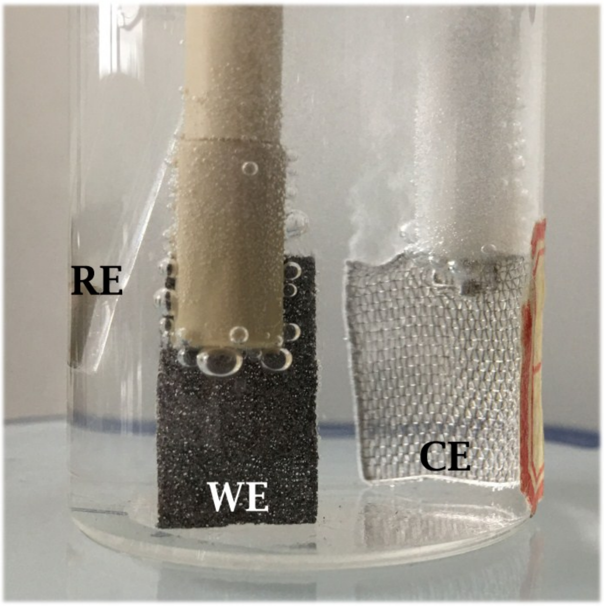

Fig. S17 Photograph of the electrolyzer during UOR catalysis.

Reference

1. J. Xie, J. Zhang, S. Li, F. Grote, X. Zhang, H. Zhang, R. Wang, Y. Lei, B. Pan, Y. Xie, J. Am. Chem. Soc. 135 (2013) 17881-17888.
2. K. Xu, H. Ding, K. Jia, X. Lu, P. Chen, T. Zhou, H. Cheng, S. Liu, C. Wu, Y. Xie, Angew. Chem. Int. Ed. 55 (2016) 1710-1713.
3. J.D. Benck, Z. Chen, L.Y. Kuritzky, A.J. Forman, T.F. Jaramillo, ACS Catal. 2 (2012) 1916-1923.
4. J. Xie, H. Zhang, S. Li, R. Wang, X. Sun, M. Zhou, J. Zhou, X.W. Lou, Y. Xie, Adv. Mater. 25 (2013) 5807-5813.
5. A.B. Laursen, P.C.K. Vesborg, I. Chorkendorff, Chem. Commun. 49 (2013) 4965-4967.